Proceedings of the 7th International Conference on Civil Structural and Transportation Engineering (ICCSTE'22)
Niagara Falls, Canada – June 05-07, 2022
Paper No. 156
DOI: 10.11159/iccste22.156

Pull-out of Basalt Fibre Pellets from Cementitious Composites

R. Elhadary[1] and M. T. Bassuoni[2*]
[1]Ph.D. Candidate, Civil Engineering, University of Manitoba,
Winnipeg, Manitoba, R3T 5V6, Canada.
Elhadare@myumanitoba.ca; mohamed.bassuoni@umanitoba.ca
[2*]Professor, Civil Engineering, University of Manitoba,
Winnipeg, Manitoba, R3T 5V6, Canada,
Tel.: +1-204-2721512

Abstract **-** This study focuses on the pull-out of basalt fibre pellets [BFP] (macro-fibre) from nano-modified (nano-silica, NS) cementitious matrices without/with micro-fibres (polyvinyl alcohol, PVA). BFP is a new form of basalt fibre strands encapsulated by a polyamide resin, with textured micro-grooves. Experimental and modelling studies were conducted to determine the BFP interfacial bonding with different cementitious matrices. The lowest BFP interfacial bond strength and de-bonding energy were observed for the reference slag-based cementitious matrix. Comparatively, using NS and PVA fibres in the cementitious composites led to noticeable enhancement of bonding with BFP, which suggests their promising potential for field applications.

Keywords**:** Basalt fibre pellets (BFP); Fibre/matrix bond; Microstructures; Finite Element Analysis (FEA).

1. Introduction

Deterioration of concrete infrastructure is commonly associated with excessive cracking due various loading, chemical and environmental schemes. The low toughness of ordinary concrete motivated the advent of high-performance fiber-reinforced cementitious composites (HPFRCC) [e.g. 1-3] to control cracking and hence extend the useful service life of infrastructural elements. HPFRCC typically exhibit ductile post-cracking behavior under tension and flexural loadings depending on key mixture design parameters. Different types of binders incorporating General Use cement (GU), slag, fly ash, nano-silica, etc. and a range (0.25 to 0.35) of water-to-binder ratios (w/b) have been used with various geometries and types of fibers (e.g. polyvinyl alcohol [PVA], steel) to produce HPFRCC [e.g. 4,5]. Different types of ultrafine nanoparticles (e.g. nano-silica) have been incorporated in HPFRCC to modify microstructure and enhance hardened properties. For instance, addition of 6% nano-silica by mass to cement-based binders without/with supplementary cementitious materials creates additional nucleation sites for precipitation of hydration products [6,7], accelerates the pozzolanic reactivity [6,8], and enhances particle packing (filler effect) in the hardened paste. Also, it reduces w/b in the paste due to water absorption into its ultrahigh surface porosity.

Many studies utilized hybrid fibre systems in HPFRCC, as their performance exceeds that of individual fibre components [e.g. 9,10]. For example, in binary-scale fibre systems, micro-fibres counteract coalescence of micro-cracks, while macro-fibres restrain the growth of macro-cracks in the matrix [11-13]. Hence, various types and sizes of metallic, synthetic, and natural fibres have been used to improve the plastic and hardened properties of HPFRCC. For instance, micro-PVA fibres have been used in cement-based composites because of their hydrophilic nature and potential for impeding nucleation of cracks in the matrix [9,14]. PVA fibres have a tensile capacity up to 1600 MPa, with a moderate modulus of elasticity (up to 66 GPa) [15]; the typical dosage of PVA micro-fibres is 2% by volume of the composite to yield a strain hardening behaviour [15]. However, there is still dearth of information on the use of PVA in various HPFRCC applications, including its interaction with other types of macro-fibres.

Macro-basalt fibres have emerged in concrete research since last decade, owing to their high tensile strength (up to 4,000 MPa), adequate modulus of elasticity (93-110 GPa), high thermal and corrosion resistances, and lower cost compared with other alternatives such as glass and carbon fibres [16-19]. While basalt fibres initially have adequate bonding with the cementitious matrix, this bond diminishes within a relatively short period of time (approximately 90 days) due to alkali-silica reactions between the pore solution and silicate component of basalt [20]. This motivated the development of a new fibre type termed basalt fibre pellets (BFP), where basalt fibre strands are encapsulated with a

polymeric resin (e.g. polyamide [21]) for protection against alkaline media. Yet, research on the use of BFP in HPFRCC is still at early stages.

For fundamental understanding of the performance of HPFRCC, characterization of fiber/matrix interaction is of outmost concern. The fiber/matrix interfacial bonding is a governing factor for bridging cracks and progressive load transfer mechanisms. The fiber type, strength, orientation, geometry, and volume fraction and matrix properties are the key parameters affecting fiber/matrix adhesion. Focused research is still needed to explore the effect of cementitious composites comprising various matrices on the BFP/matrix interfacial bonding characteristics. Such data is crucial to identify the functionality of these composites for safe and resilient use in various applications. Hence, the primary objective of the current study was to evaluate the interaction of BFP with different nano-modified (nano-silica) cementitious matrices comprising high volume-slag without/with micro- PVA fibers using integrated experimental (single pellet pull-out/microstructure) and modeling (homogenization/FEM) approaches.

2. Experimental Program

2.1 Materials and Mixtures

General use cement (GU) and Grade 100 slag meeting CSA-A3001 [22] requirements were used as the main components of the base binder (700 kg/m^3). Nano-silica (6%) was added to the base binder in the composites. The NS solution comprises 50% SiO_2 particles well dispersed in an aqueous solution, with a specific surface area of 80,000 m^2/kg, mean particles size of 35 nm, and density of 1.1 g/cm^3. It was reported that 6% of this NS solution had a positive effect at improving the pore structure and hardened properties of concrete comprising supplementary cementitious materials [8,21].

Fine aggregate with continuous gradation of 0 to 600 μm was used in the mixtures, and its fineness modulus, absorption and specific gravity were 2.9, 1.5% and 2.6, respectively. In order to improve the workability of all mixtures, poly-carboxylic high-range water reducer (HRWR), complying with ASTM C494 Type F [23], was used at a dosage of 100 to 150 ml per 10 kg of binder to achieve a constant flow table diameter of 180±20 mm. Two different types and sizes of fibres [**Table 1]** were used to reinforce the mixtures: PVA (micro-fibres) and BFP (macro-fibres) [**Figure 1**].

Table 1: Properties of fibres

Property	PVA	BFP
Length (mm)	12	36
Diameter/width (mm)	38×10^{-3}	1.8
Aspect ratio	315	20
Specific gravity	1.3	1.7
Tensile strength (MPa)	1600	2,300
Elastic modulus (GPa)	66	65

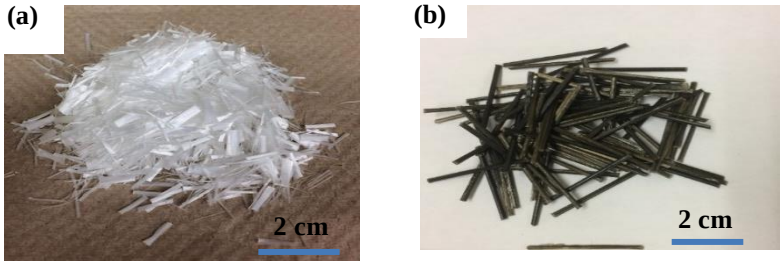

Figure 1: Fibre types: (a) PVA, and (b) BFP.

Three mixtures were prepared at 0.30 w/b with 50% cement and 50% slag (base binder: 700 kg/m^3) meeting the requirement for high-volume supplementary cementitious materials (HVSCM-1) concrete in Annex K, CSA 23.1 [24].

Nano-modified binders comprised 6% NS without/with 1% PVA by volume of composite. The proportions of all mixtures are listed in **Table 2**. For the mixture IDs, the letters G, N, and V refer to slag, nano-silica, and polyvinyl alcohol fibres, respectively, while the numbers indicate the dosage of PVA fibre.

Table 2: Mixtures proportions per cubic meter

Mixture ID	Cement (kg)	Slag (kg)	Water* (kg)	NS (kg)	Fine Aggregate (kg)	PVA (kg)	HRWR (l)
G	350	350	210	--	1352	--	5.3
G-N	350	350	180	84	1231	--	5.5
G-N-V1	350	350	180	84	1205	13	11

*Adjusted amount of mixing water considering the water content of NS (50% solid content).

The NS sol was directly dispersed into the mixing water using a homogenizer at 2,000 rpm for 4 min. Initially, the dry constituents (sand, cement, slag) were added to a concrete pan mixer (60 rpm), followed by gradual addition of required mixing water containing NS sol with half the amount of HRWR while constantly mixing until the homogeneity of the mixture was achieved. PVA fibres were added last with the remaining amount of HRWR, and the ingredients were mixed for additional 8 to 10 min to achieve uniform distribution of fibres. After casting the composites in moulds, all specimens were consolidated using a vibrating table. Polyethylene sheets were used to cover the surface of the specimens for 24 h. Subsequently, the specimens were demoulded and cured in a standard room maintained at a 22±2°C and a relative humidity of more than 95% until testing.

2.2 Tests

The single pellet pull-out test was conducted at 56 days through testing six replicate blocks (100×100×50 mm) including a single BFP, with an embedded length of 18 mm in the middle of the blocks, with 0.2 mm/min displacement rate [25]. Microstructural tests were performed to corroborate the trends obtained from the single pellet test. Scanning electron microscopy (SEM) with elemental dispersive X-ray (EDX) was carried out at 56 days on extracted pieces comprising BFP alone or coupled with PVA fibres to capture morphological features at the interface. The samples were coated with carbon to improve their conductivity for imaging.

3. Finite Element Modelling

3.1. Phase I: Homogenization Method

Based on computational non-linear homogenization method, cubic representative volume elements (RVEs) were developed herein in ANSYS R19.2 workbench [26] to determine the homogenized stiffness coefficients k_{ij} for matrices with inclusions/fibers (i.e. G-N-V1). **Figure 2** shows homogenized RVE with cubic dimensions of 12 mm. Each meso-scale RVE includes the matrix and randomly distributed micro-fibres (PVA fibres) oriented randomly in space (*x*, *y*, *z*), assuming anisotropic properties. RVE were modelled with a mesh size of 100 µm, and thus the total number of elements were 15170. The elements were subjected to uniaxial tensile stress and shear deformation along the principal coordinates to determine the components of k_{ij} (**Eq. 1**) for different boundary conditions/matrices interacting with BFP through periodic boundary condition displacement on RVE boundaries, where, k_{ij} is the effective tensor modulus of homogenized stiffness matrix, $d\sigma_{ij}$and $d\varepsilon_{ij}$ are the volume averaged stress and strain tensors of the RVE, respectively, and *i* and *j* are equal to 1, 2 or 3 with respect to the global axes *x*, *y*, and *z*, respectively.

$$d\sigma_{ij} = k_{ij}\, d\varepsilon_{ij} \tag{1}$$

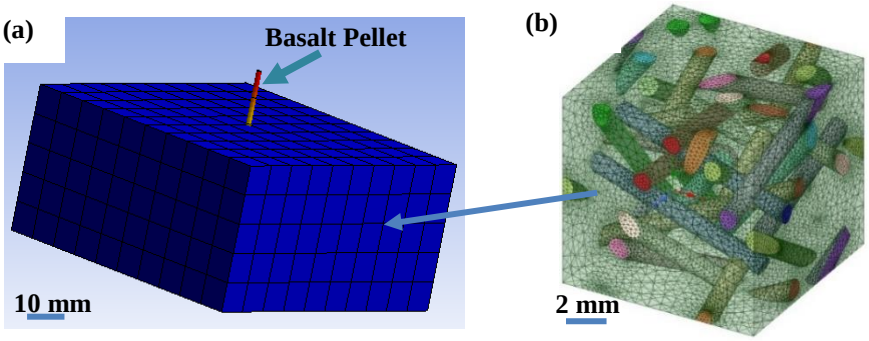

Figure 2: Homogenization RVEs: a macro-RVE scale, and (b) meso-RVE of mixture G-N-V1

3.2. Phase II: Finite Element Analysis

The BFP was modelled as a linear-elastic media using LINK8 element, which is a 3D spar (bar) element defined by two nodes with three translational degrees of freedom at each node. The matrix block surrounding BFP was modelled as non-linear elastic media by SOLID65 brick element, with eight nodes located at corners; each node has three translational degrees of freedom in the *x*, *y*, and *z* directions. The specific gravity, Young's modulus, and maximum tensile strength for BFP were 1.74 kg/m^3, 65 GPa and 2300 MPa, respectively (**Table 1**). The Poisson's ratio for BFP and cementitious matrices were taken as 0.3 and 0.2, respectively. The input parameters for all matrices included the tensile stress-strain relationships, Young's modulus and peak stress and strain were obtained experimentally using a quasi-static direct tension test (**Figure 3**). The block model was simulated with dimensions of 100×100×50 mm including a single pellet embedded at a length 18 mm and diameter of 1.8 mm in the middle of the block. The movement of block was restrained by fixing the bottom, and the displacement rate of the applied load was 0.2 mm/min at to the free end of the BFP similar to the experimental scheme. The model was meshed with a mesh size of 10 mm resulting in a total of 2660 nodes and 922 elements. The interfacial behaviour between the pellet and cementitious matrices was modelled as a bonded pair using CONTA175 and TARGE170 by CZM governed by a bilinear-mode-II, with a total of 408 contact elements.

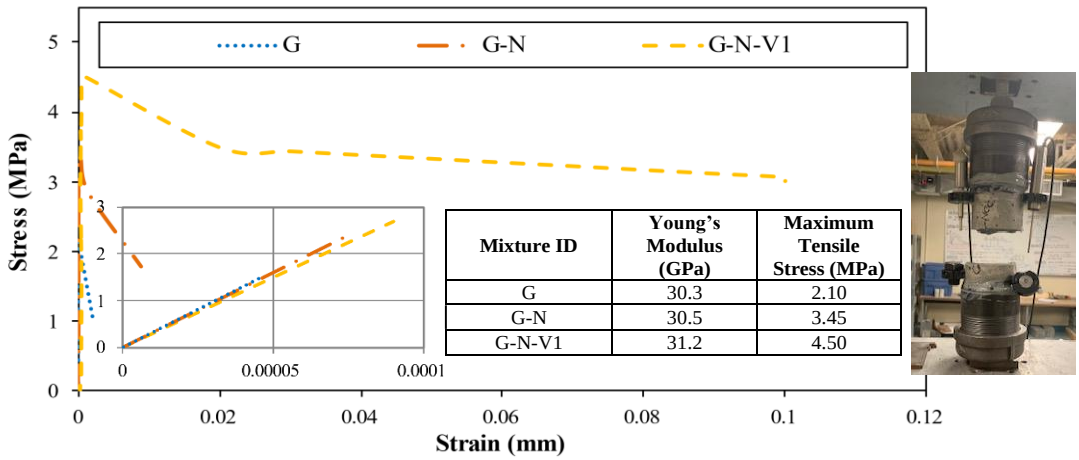

Mixture ID	Young's Modulus (GPa)	Maximum Tensile Stress (MPa)
G	30.3	2.10
G-N	30.5	3.45
G-N-V1	31.2	4.50

Figure 3: Tensile stress-strain relationships of the different matrices.

4. Results and Discussion

4.1. Experimental

Figure 4 show the BFP pull-out process from the different matrices. The matrix comprising NS had improved interfacial bonding with BFP. For instance, the pull-out strength of BFP from G-N and its de-bonding energy was 27% and

11%, respectively higher than that of the reference matrix without nano-silica (G). SEM analysis showed that unlike the reference matrix (G), the inclusion of 6% NS led to extensive deposition of cementitious gel/products in the BFP micro-groves (e.g. **Figure 5**) cross-linking the pellet with matrix. This led to high contact surface area between BFP and matrix and consequently enhancement in BFP/matrix friction and interfacial bonding. The average *Ca/Si* of the paste at the interface between BFP and G-N was 1.18 compared to 1.7 in primary/hydration process [27], substantiating efficient filling effect and pozzolanic reactivity of the former resulting in the participation of additional and stiffer pozzolanic C-S-H in the contact zone with BFP.

Adding 1% of PVA fibres led to further improvement of the resistance of BFP to pull-out from the NS-modified cementitious matrix; the pull-out strength and de-bonding energy of G-N-V1 were 25% and 46%, respectively higher than that of mixture G-N (**Figure 4)**. PVA micro-fibres in the matrix could control the nucleation and coalescence of micro-cracks. PVA fibres create hydrogen bonds between molecules forming new compounds at the boundaries with cement paste (chemical effect) [14], resulting in compact structure around BFP. Also, randomly distributed micro-PVA clusters in the paste surrounding BFP [e.g. **Figure 6**], increased the chance of interlocking, friction, and in turn bonding capacity.

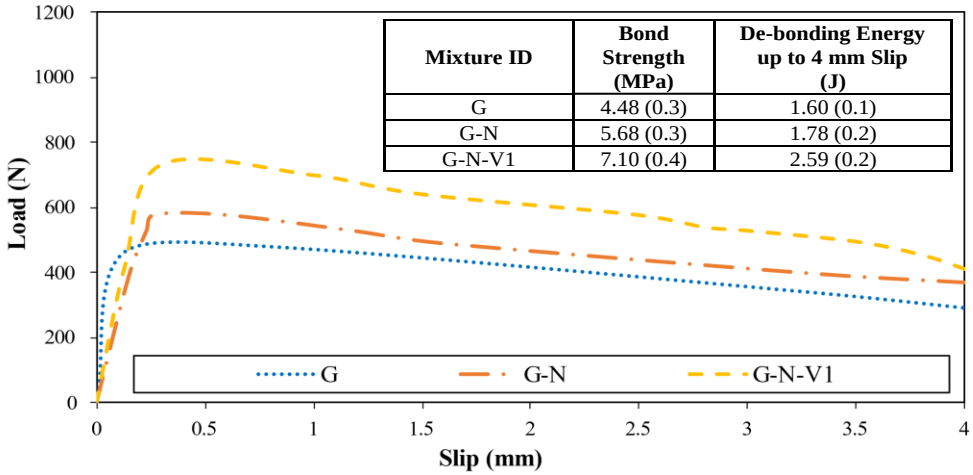

Mixture ID	Bond Strength (MPa)	De-bonding Energy up to 4 mm Slip (J)
G	4.48 (0.3)	1.60 (0.1)
G-N	5.68 (0.3)	1.78 (0.2)
G-N-V1	7.10 (0.4)	2.59 (0.2)

Figure 4: Bond-slip relationships from the single pellet pull-out tests.

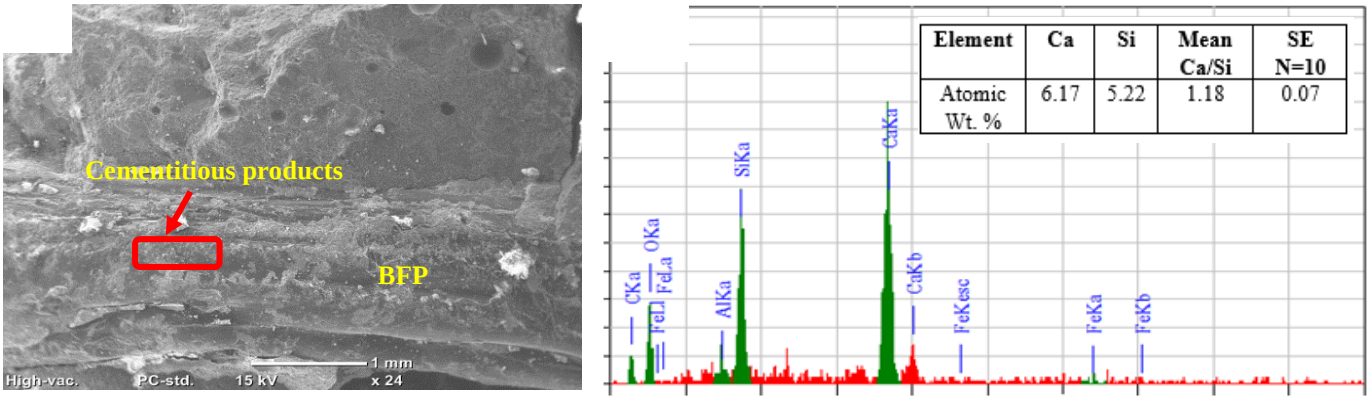

Element	Ca	Si	Mean Ca/Si	SE N=10
Atomic Wt. %	6.17	5.22	1.18	0.07

Figure 5: Exemplar SEM micrograph for matrix G-N at 56 days: (a) ITZ with BFP, and (b) EDX spectrum of paste at the indicated location in (a). (SE = standard error for 10 points).

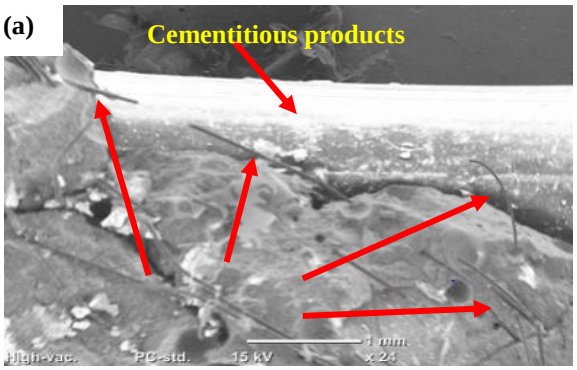

Figure 6: Exemplar SEM micrographs at 56 days showing interaction of BFP with G-N-V1.

4.2. Modeling Results

The modelling results conformed to the experimental trends. The predicted pull-out strength of BFP from G-N and its de-bonding energy were 13% and 18%, respectively higher than that from the reference matrix (G). This was ascribed to the role of NS in producing extensive deposition of cementitious products in the BFP micro-groves as discussed earlier. Moreover, inclusion of 1% micro-PVA fibres in the matrix modified with NS (G-N-V1) achieved the highest estimations for bonding strength and de-bonding energy compared with that of the other mixtures (**Table 3**), owing to the clustering, interlocking and friction effects of well distributed micro-PVA around BFP. Parametric analysis showed that the bond strength and de-bonding energy for the mixture incorporating 2% PVA fibres with BFP would increase by 29% and 33%, respectively compared with that of the mixture comprising 1% of PVA fibres [**Figures 7(a) and (b)**]. **Equation 2** shows the results of k_{ij} for a 12 mm RVE. The coupling terms for k_{ij} indicated that the value of extension-shear and shear-shear components were much lower than that of the extension-extension component, and thus they were negligible.

$$k_{ij} = \begin{bmatrix} \text{Extension-Extension} & & & \text{Shear-Extension} & & \\ 31.232 & 23.910 & 23.125 & 0.07 & 0.09 & 0.32 \\ & 31.231 & 23.185 & 0.02 & -0.1 & 0.17 \\ & & 31.233 & -0.03 & 0.02 & 0.28 \\ & & & 14.644 & 0.03 & 0.02 \\ & \text{Symmetry} & & & 14.644 & 0.01 \\ & & & & \text{Shear-Shear} & 14.64 \end{bmatrix} \quad (2)$$

Table 3: Experimental versus modelling results for the single pellet pull-out tests

Mixture ID	Bond Strength (MPa)		Error (%)	De-bonding Energy up to 4 mm Slip (J)		Error (%)
	Experimental	Modelling		Experimental	Modelling	
G	4.48	4.73	6	1.60	1.59	1
G-N	5.68	5.34	6	1.78	1.87	5
G-N-V1	7.10	6.87	3	2.59	2.35	10

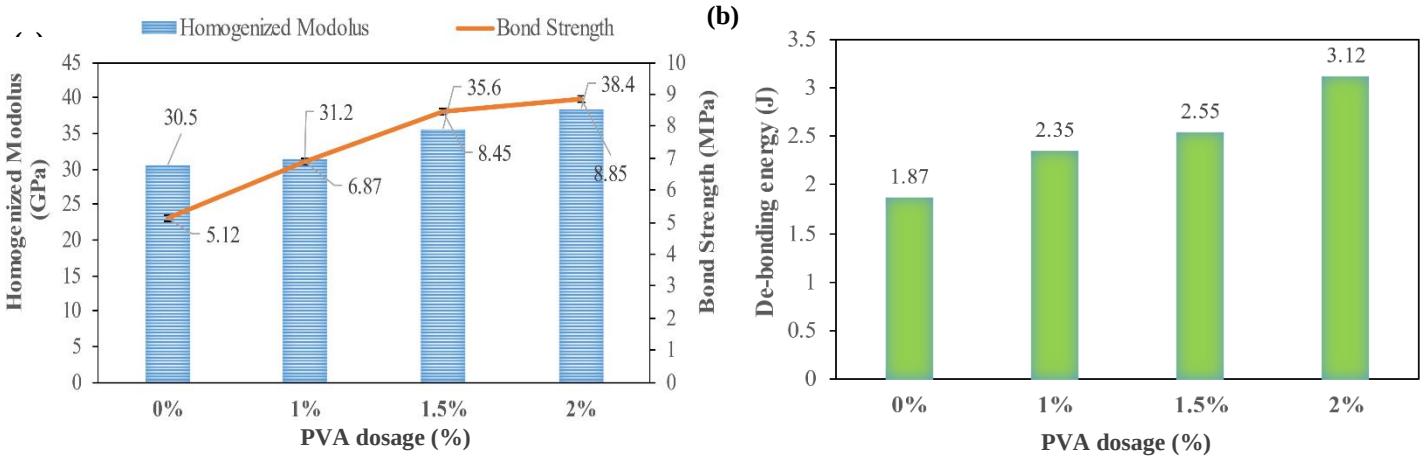

Figure 7: Parametric analysis results: (a) homogenized modulus and bond strength of mixture G-N reinforced with PVA, and (b) debonding energy.

5. Conclusions

Based on types of matrices and experimental/modelling approaches implemented in this study, the following conclusions can be drawn:

- Nano-modified cementitious composites incorporating 6% NS (G-N) had balanced performance in terms of enhancing the BFP interfacial bond (by 27%) and de-bonding energy (by 11%) relative to that of the reference binder (G). This was attributed to the synergetic effects of NS with slag, which increased the degree of matrix maturity, produced dense microstructure, led to extensive deposition of cementitious gel/products in the BFP micro-groves and consequently enhancement of BFP/matrix friction and interfacial bonding.
- The randomly distributed micro-PVA clusters in the G-N paste surrounding BFP promoted the likelihood of interlocking, which increased friction, bond strength and de-bonding energy (highest values of 7.1 MPa and 2.59 J for matrix G-N-V1 in the single pellet pull-out tests), which suggests the promising potential of these composites for field applications.
- The FEM approach was reliable at modeling the pull-out behaviour of BFP, with less than 10% error. The parametric analysis indicated that BFP interfacial bond strength and de-bonding energy could be improved (29% and 33%, respectively) by increasing the content of PVA from 1% to 2% in the G-N matrix.

Acknowledgements

The authors highly appreciate the financial support from Natural Sciences and Engineering Research Council of Canada (NSERC RGPIN 2020/2025), and University of Manitoba Research Grants Program (URGP-2019/2020) to conduct this study under the theme: resilient high-performance materials for sustainable infrastructure.

References

[1] I.H. Yang, C. Joh, and B.S. Kim, "Structural behavior of ultra-high performance concrete beams subjected to bending," *Engineering Structures*, Vol. 32, no. 11, pp.3478-3487,2010.

[2] R. Ranade, V.C. Li, M.D. Stults, T.S. Rushing, J. Roth, and W.F. Heard, "Micromechanics of high-strength, high-ductility concrete," *ACI Materials Journal*, Vol. 110, no. 4, pp. 375-384, 2013.

[3] M.J. Bandelt, and S.L. Billington, "Impact of reinforcement ratio and loading type on the deformation capacity of high-performance fiber-reinforced cementitious composites reinforced with mild steel," *Journal of Structural Engineering*, Vol. 142, no. 10, pp. 040160840-0401608414, 2016.

[4] D. Meng, T. Huang, Y.X. Zhang, and C.K. Lee, "Mechanical behaviour of a polyvinyl alcohol fibre reinforced engineered cementitious composite (PVA-ECC) using local ingredients," *Construction and Building Materials*, Vol. 141, pp. 259-270, 2017.

[5] Z. Pan, C. Wu, J. Liu, W. Wang, and J. Liu, "Study on mechanical properties of cost-effective polyvinyl alcohol engineered cementitious composites (PVA-ECC)," *Construction and Building Materials*, Vol. 78, pp. 397-404, 2015.
[6] D. Kong, X. Du, S. Wei, H. Zhang, Y. Yang, and S.P. Shah, "Influence of nano-silica agglomeration on microstructure and properties of the hardened cement-based materials," *Construction and Building Materials*, Vol. 37, pp. 707-715, 2012.
[7] A.M. Said, M.S. Zeidan, M.T. Bassuoni, and Y. Tian, "Properties of concrete incorporating nano-silica," *Construction and Building Materials*, Vol. 36, pp. 838-844, 2012.
[8] A. Ghazy, M.T. Bassuoni, and A. Shalaby, "Nano-modified fly ash concrete: a repair option for concrete pavements," *ACI Materials Journal*, Vol. 113, no. 2, pp. 231-242, 2016.
[9] E.T. Dawood, and M. Ramli, "High strength characteristics of cement mortar reinforced with hybrid fibres," *Construction and Building Materials*, Vol. 25, no.5, pp. 2240-2247, 2011.
[10] S.H. Park, D.J. Kim, G.S. Ryu, and K.T. Koh, "Tensile behavior of ultra-high-performance hybrid fiber reinforced concrete," *Cement and Concrete Composites*, Vol. 34, no. 2, pp. 172-184, 2012.
[11] C. Zhang, and M. Cao, "Fiber synergy in multi-scale fiber-reinforced cementitious composites," *Journal of Reinforced Plastics and Composites*, Vol. 33, no. 9, pp. 862-874, 2014.
[12] B.S. Sindu, and S. Sasmal, "On the development and studies of nano-and micro-fiber hybridized strain hardened cementitious composite," *Archives of Civil and Mechanical Engineering*, Vol. 19, no. 2, pp. 348-359, 2019.
[13] R. Elhadary, and M.T. Bassuoni, "Mechanical properties of nano-modified cementitious composites reinforced with single and hybrid Fibers," *Transportation Research Record*, Vol. 2675, no. 9, pp. 56-64, 2021.
[14] S.G. Liu, C. He, C.W. Yan, and X.M. Zhao, "Water permeability of polyvinyl alcohol (PVA) fiber reinforced cementitious composites," *Advanced Materials Research*, Vol. 150, pp. 1009-1012, 2011.
[15] V.C. Li, S. Wang, C. Wu, "Tensile strain-hardening behavior of polyvinyl alcohol engineered cementitious composite (PVA-ECC)," *ACI Materials Journal*, Vol. 98, no. 6, pp. 483-492, 2001.
[16] T. Ayub, N. Shafiq, and M.F. Nuruddin," Mechanical properties of high-performance concrete reinforced with basalt fibers," *Procedia Engineering*, Vol. 77, pp. 131-139, 2014.
[17] P. Iyer, S.Y. Kenno, and S. Das, "Mechanical properties of fiber-reinforced concrete made with basalt filament fibers," *Journal of Materials in Civil Engineering*, Vol. 27, no. 11, pp. 040150151-040150158, 2015.
[18] M.E. Arslan, "Effects of basalt and glass chopped fibers addition on fracture energy and mechanical properties of ordinary concrete: CMOD measurement," *Construction and Building Materials*, Vol. 114, pp. 383-391, 2016.
[19] P. Iyer, S.Y. Kenno, and S. Das, "Performance of Fiber-Reinforced Concrete Made with Basalt-Bundled Fibers. *Advances in Civil Engineering Materials*, Vol. 5, no. 1, pp. 107-123, 2016.
[20] C. Jiang, K. Fan, F. Wu, and D. Chen, "Experimental study on the mechanical properties and microstructure of chopped basalt fibre reinforced concrete," *Materials and Design*, Vol. 58, pp. 187-193, 2014.
[21] K. Mahmoud, A. Ghazy, M.T. Bassuoni, and E. El-Salakawy," Properties of nanomodified fiber-reinforced cementitious composites," *Journal of Materials in Civil Engineering*, Vol. 29, no. 10, pp. 04017173-040171712, 2017.
[22] CSA (Canadian Standard Association) CAN/CSA-A3001: Cementitious materials for use in concrete, Canadian Standards Association (CSA), Mississauga, Ontario, Canada, 2018.
[23] ASTM C494/C494M: Standard specification for chemical admixtures for concrete, ASTM International, West Conshohocken, PA, USA, 2017.
[24] CSA (Canadian Standard Association) CSA-A23.1/A23.2: Concrete materials and methods of concrete construction/test methods and standard practices for concrete, Canadian Standard Association (CSA), Mississauga, Ontario, Canada, 2019.
[25] A. Azzam, M.T. Bassuoni, and A. Shalaby," Nanomodified Cementitious Composites Incorporating Basalt Fiber Pellets under Tensile and Impact Loads," *Journal of Materials in Civil Engineering*, Vol. 33, no. 10, pp. 04021260-040212614, 2021.
[26] ANSYS Inc, Ansys Workbench 19 R2. United States, Pennsylvania, 2020.

[27] R. Detwiler, J. Bhatty, and S. Bhattacharja, “Supplementary cementing materials for use in blended cements,” *Portland Cement Association*. United States: Illinois, Skokie, 1996.